Thienylsilane-Modified Indium Tin Oxide as an Anodic Interface in Polymer/Fullerene Solar Cells

David A. Rider,[†] Ken D. Harris,[‡] Dong Wang,[‡] Jennifer Bruce,[‡] Michael D. Fleischauer,[‡] Ryan T. Tucker,[§] Michael J. Brett,*[,‡,§] and Jillian M. Buriak*[,†,‡]

Department of Chemistry, University of Alberta, 11227 Saskatchewan Drive, Edmonton, Alberta T6G 2G2, Canada, National Institute for Nanotechnology, 11421 Saskatchewan Drive, Edmonton, Alberta T6G 2M9, Canada, and Department of Electrical and Computer Engineering, University of Alberta, Edmonton, Alberta T6G 2V4, Canada

ABSTRACT The generation and characterization of a robust thienylsilane molecular layer on indium tin oxide substrates was investigated. The molecular layer was found to reduce the oxidation potential required for the electrochemical polymerization of 3,4-ethylenedioxythiophene. The resulting electrochemically prepared poly(3,4-ethylenedioxythiophene):poly(*p*-styrenesulfonate) (ePEDOT:PSS) films were found to be more uniform in coverage with lower roughness and higher conductivity than analogous films fabricated with bare ITO. A relative improvement in the efficiency of 2,5-diyl-poly(3-hexylthiophene) (P3HT)/[6,6]-phenyl-C_{61}-butyric acid methyl ester (PCBM) bulk heterojunction solar cells was observed when devices were formed on thienylsilane-modified ITO electrodes, rather than unmodified ITO control electrodes.

KEYWORDS: photovoltaic solar cell • thiophene molecular layer • PEDOT:PSS • bulk heterojunction • electrochemical deposition

INTRODUCTION

Organic solar cells (1−16) are an attractive alternative to their conventional silicon-based counterparts largely due to superior processing conditions, processing speed, and cost (17−20). A widely researched organic solar cell employs a two-component active layer consisting of an electron-donating conjugated polymer and an electron-accepting fullerene structured in a disordered bicontinuous interpenetrating network configuration known as the bulk heterojunction (BHJ) (21−26). A typical BHJ polymer organic photovoltaic device (OPV) solar cell consists of an active layer of regioregular 2,5-diyl-poly(3-hexylthiophene) (P3HT) and [6,6]-phenyl-C_{61}-butyric acid methyl ester (PCBM) (27, 28), although promising low-band-gap polymer analogues are currently being developed (18, 29−32). A schematic drawing of a typical BHJ device is provided in Figure 1. In these excitonic OPVs, the absorption of light generates bound electron−hole pairs (i.e., excitons) which ideally dissociate with high yield into free charge carriers at donor−acceptor interfaces. The free electron and hole charge carriers consequently migrate from the interface to the cathode (e.g., a reflective metal such as Al) and the anode (e.g., a transparent conducting oxide, such as indium tin oxide (ITO)), respectively.

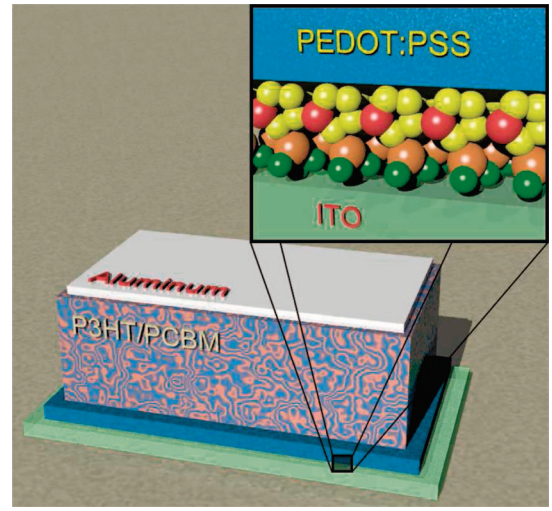

FIGURE 1. Schematic depiction of a bulk heterojunction photovoltaic device: red atoms, S; yellow atoms, C; orange atoms, Si; green atoms, O. In the active region, donor and acceptor materials (in this case P3HT/PCBM) are phase-segregated on a nanometer scale and an extremely large interfacial surface area is achieved. Charge transfer between the active regions and electrodes is potentially improved by adding an interfacial molecular layer (inset).

In spite of tremendous advances in both the understanding and fabrication of OPV solar cells (19, 21, 33−35), global commercialization remains limited due to poor performance and stability (36, 37) and has therefore been the topic of recent research (38−41). Several publications unequivocally state that improved charge transfer across material interfaces, especially between the active layers and their associated electrodes, is critical to addressing many fundamental issues and that interfacial modification layers are essential to the achievement of acceptable device performance

* To whom correspondence should be addressed. E-mail: brett@ece.ualberta.ca (M.J.B.); jburiak@ualberta.ca (J.M.B.).
Received for review September 26, 2008 and accepted October 10, 2008
[†] Department of Chemistry, University of Alberta.
[‡] National Institute for Nanotechnology.
[§] Department of Electrical and Computer Engineering, University of Alberta.
DOI: 10.1021/am800081k

(42−44). Reduced contact resistance at the conductor/active layer interface is expected to create an overall reduction in device series resistance, thereby improving the energy extraction efficiency (45, 46). To this end, elegant research has recently shown that application of oligosiloxanes to anodes for OLEDs permits optimization of charge injection (47), whereas the use of alkylthiophenes (48, 49) and alkylterthiophenes (50) improves anodic charge extraction in OPV devices. Poly(3,4-ethylenedioxythiophene):poly(*p*-styrenesulfonate) (PEDOT:PSS) is a polymer blend of cationic and conducting PEDOT that is charge-balanced by anionic and insulating PSS. This material has been widely employed as an OPV hole-collecting interfacial layer at the anode due to its stable and high work function and electron-blocking properties (51). A PEDOT:PSS interfacial layer leads to a smoother electrode with improved ohmic contact with the active layer, enhanced hole collection (52, 53), and increased open-circuit voltage (V_{oc}) (53) as well as improved areal electrical uniformity in completed devices (54). Typically PEDOT:PSS is applied to ITO electrodes by spin-coating from inhomogeneous aqueous dispersions, yielding films with considerable structural, morphological, and electrical nonuniformity (55−59). As-cast PEDOT:PSS films have been shown to undergo a complex phase separation leading to PSS-enriched surfaces with dramatically reduced orthogonal-to-plane conductivity (60, 61). The application of a thienylsilane interfacial layer for the electrochemical coating of PEDOT:PSS films on ITO anodes and subsequent application in BHJ polymer OPV solar cells remains relatively unexplored.

Herein we discuss the formation and characterization of a robust thienylsilane molecular layer on an ITO electrode (see inset in Figure 1). These surface-functionalized electrodes were subsequently used in standard electrochemical cells for the electrodeposition of PEDOT:PSS (ePEDOT:PSS). It was found that highly conductive films could be produced at oxidative potentials well below that of the bare ITO case. A series of BHJ OPV solar cells was fabricated with ePEDOT:PSS, and it was found that thienylsilane interfacial layers significantly improved the resulting short circuit current density and device efficiency compared to those prepared under identical conditions with unfunctionalized ITO.

EXPERIMENTAL SECTION

Reagents and Physical Measurements. Triethoxy-2-thienylsilane, 3,4-ethylenedioxthiophene, sodium poly(*p*-styrenesulfonate) ($M_w \approx 1\,000\,000$ Da), toluene, chlorobenzene, methanol, and pentane were used as received from Sigma-Aldrich. Regioregular 2,5-diyl-poly(3-hexylthiophene) and [6,6]-phenyl-C_{61}-butyric acid methyl ester were used as received from Rieke Metals and American Dye Source Inc., respectively. Indium tin oxide coated glass substrates (8−12 Ω/□) were acquired from Delta Technologies, Ltd. The ITO-coated glass substrates were cleaned by sequential 10 min ultrasonication in dichloromethane, water, and isopropyl alcohol. Prior to use, ITO-coated glass substrates were further cleaned by exposure to a 10 min air plasma at ∼0.1 mTorr (Harrick Plasma, PDC 32G, 18W).

Cyclic voltammetry was carried out using a Princeton Applied Research Model 2273 potentiostat employing various ITO substrates as the working electrodes (area ∼1.5 cm^2) in a standard three-electrode electrochemical cell. All potentials were measured and are reported relative to a Ag/Ag^+ reference electrode recorded at a scan rate of 100 mV/s. Surfaces were characterized by scanning force microscopy (SFM), scanning electron microscopy (SEM), X-ray photoelectron spectroscopy (XPS), and Kelvin probe. SEM and XPS were performed under high-vacuum conditions ($<10^{-5}$ Pa). A Nanoscope IV (Digital Instruments/Veeco) instrument, operated in tapping mode with commercially available Si cantilevers (Micromash, frequency 300 kHz), was used for SFM. Conductivity measurements of ePEDOT:PSS films were carried out by conductive probe SFM (CP-SFM) in contact mode with Pt-coated SFM tips (Micromash). SEM (Hitachi S-4880 FE-SEM) was typically performed with an accelerating voltage of 10 keV. XPS (Kratos Analytical, Axis-Ultra) was performed using monochromatic Al Kα X-ray irradiation at a photon energy of 1486.6 eV. The instrument was calibrated using the C 1s signal (BE = 284.9 eV).

Work functions were measured using a KP Technology Ltd. SKP Kelvin probe. In the Kelvin probe arrangement, the test sample is electrically connected to an oscillating electrode which oscillates above the sample. The sample and vibrating electrode form the two plates of a parallel plate capacitor. Due to the varying plate spacing, an alternating current flows which depends upon the work function difference between sample and vibrating tip. This current flow, recorded at various backing voltages, is used to extract the relative work function difference between sample and vibrating tip (62). For absolute magnitudes, a reference sample with a known work function must also be measured using the same vibrating tip in the same environment. In this case, we chose a freshly prepared highly oriented pyrolytic graphite (HOPG) reference (63).

Modification of ITO Substrates with Triethoxy-2-thienylsilane. Cleaned ITO-coated glass substrates were evacuated for 30 min in a desiccator containing an open vessel of triethoxy-2-thienylsilane (∼0.1 mL). Substrates were left under static vacuum for 18 h and then exposed to ambient atmosphere for 2 h prior to use.

Photovoltaic Device Fabrication. The bulk heterojunction polymer/fullerene photovoltaic devices consisted of blended films of regioregular P3HT and PCBM sandwiched between a transparent anode and a reflective cathode. The anode consisted of an ITO-coated glass substrate electrochemically modified with poly(3,4-ethylenedioxythiophene):poly(*p*-styrenesulfonate) (ePEDOT:PSS). A potentiostatic method (applied potential 1.15 V) was used for the electrochemical deposition of ePEDOT:PSS on the anode. Film thickness was controlled by monitoring the electrical charge passed during the growth process. After polymerization, the ePEDOT:PSS films were thoroughly and sequentially rinsed with deionized water (18 MΩ), methanol, and pentane followed by drying under vacuum (<0.1 Pa) for 30 min at room temperature. P3HT was dissolved in chlorobenzene to make a 10 mg/mL solution, followed by blending with a 0.8 equiv mass of PCBM. The blend was stirred for 14 h at 50 °C in a glovebox before spin casting. The P3HT/PCBM solution was applied by spin coating from chlorobenzene solution at 700 rpm followed by annealing under an inert atmosphere (Ar-equipped glovebox, <5 ppm of O_2 and H_2O) at 150 °C for 30 min. The cathode consisted of 120 nm of Al and was applied by thermal evaporation under high-vacuum conditions ($<10^{-4}$ Pa).

Photovoltaic device testing was done at ambient atmosphere and temperature under simulated AM 1.5G irradiation using a xenon-lamp-based solar simulator (Oriel 91191 1000W Solar Simulator), with a nominal device irradiation of 100 mW/cm^2. The actual irradiance at our test position used for all experiments was calibrated using an NREL-calibrated reference cell of known efficiency (12% efficiency at 25 ± 1 °C) and found to be 95 mW/cm^2.

Scheme 1. Procedure for the Chemisorptive Functionalization of ITO-Coated Glass with Triethoxy-2-thienylsilane and the Subsequent Electrochemical Preparation of ePEDOT:PSS

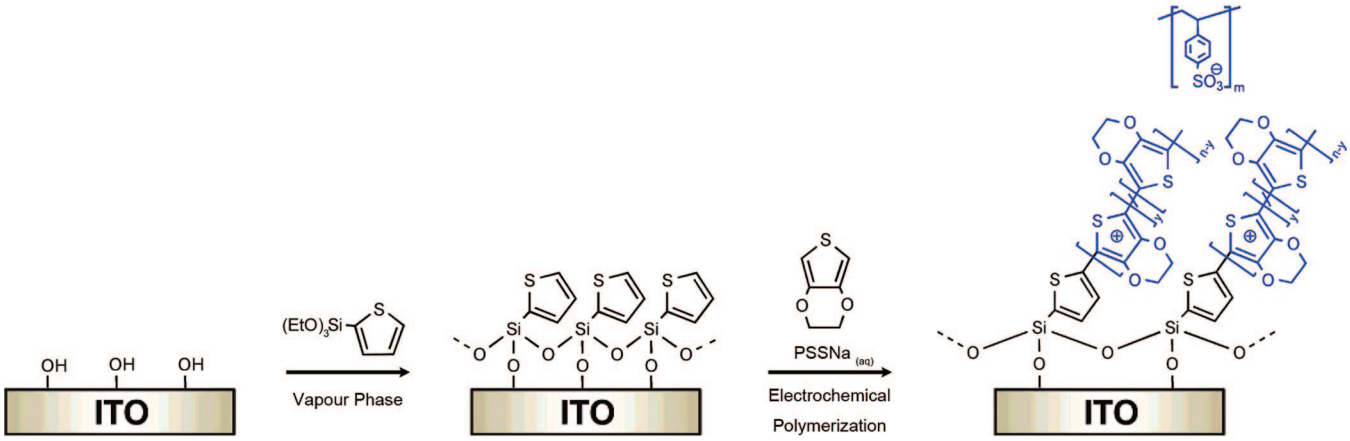

RESULTS AND DISCUSSION

In an effort to enhance the wetting, electrical contact, and adhesion of PEDOT:PSS on the transparent conducting oxide anodes (64) in photovoltaic solar cells, we investigated the formation of a robust thienylsilane molecular layer from the hydrolysis of triethoxy-2-thienylsilane on hydroxy-functionalized indium tin oxide (ITO) substrates. Unique to this study, the resulting interfacial layer would lack alkyl tethers that would otherwise impart a significant dielectric and insulating character between the ITO surface and thienyl moieties. Recently, Armstrong et al. examined the generation and chemical nature of various hydroxy-functionalized ITO surfaces (65). Through the use of hydrogen-bonding interactions with ferrocenedicarboxylic acid, it was found that an air plasma was a very effective route to a high areal density of electroactive surface hydroxyl groups. Following these results, we treated the ITO substrates with this protocol for generating an appropriate electroactive surface for the electrochemical deposition of thiophene-based films (66).

Molecular Layer Synthesis. As shown in Scheme 1, a molecular layer of triethoxy-2-thienylsilane is chemisorbed from the vapor phase onto clean, hydroxy-functionalized ITO. The generation of a thiophene-bearing siloxane layer occurs through the reaction of ethoxysilyl groups with surface-bound hydroxyl groups as well as physically adsorbed water (67). Additional hydrolysis by exposure of the surface to ambient air ensures the complete reaction of trace ethoxysilyl groups (68).

Molecular Layer Characterization. The functionalized ITO was characterized using the water contact angle, X-ray photoelectron spectroscopy (XPS), and a Kelvin probe. Following oxidation by air plasma, the ITO surface was found to be hydrophilic with a water contact angle of approximately 6°. This value agrees with recent studies for plasma-cleaned ITO surfaces (69). By Kelvin probe the work function of the ITO-coated glass was found to be 5.05 eV, a value that correlates well with those found in previous studies (70).

The surface functionalization with triethoxy-2-thienylsilane is expected to alter the chemical nature and energetics of the ITO surface. By the procedure discussed above, a thienylsilane-modified ITO interface was produced. The modified surface exhibited a significant change in hydrophilicity, where a water contact angle of ~75.5° was determined. Similar hydrophobicity was found for pyrrolyl molecular layers on ITO (71). Moreover, the water contact angle of the substrate was found to be constant over periods of up to 1 month. Angle-resolved X-ray photoelectron spectroscopy (AR-XPS) was used to probe the nature of the molecular layer on the ITO surface. This technique, where the angle between the sample surface and the detector (the takeoff angle) is varied, allows for depth profiling and is useful for the characterization of the uppermost surface (72). Summarized in Table 1 are the atomic compositions determined for In, Sn, O, C, S, and Si as a function of the takeoff angle. The table clearly identifies two trends. With decreasing takeoff angle, the intensities of indium and tin signals decrease whereas signals for the elements in the thienylsilane molecular layer (i.e., sulfur, carbon, and silicon) increase. These findings are consistent with an ITO surface bearing a molecular layer of thiophene. Shown in Figure 2a–d are the high-resolution O(1s), C(1s), S(2p), and Si(2p) XPS spectra acquired from a thienylsilane-modified ITO sample at a takeoff angle of 15°. The spectra are consistent with previous results for thiophene bearing self-assembled molecular layers (73). It is worth noting that the C(1s) and S(2p) spectra show little evidence of oxidation (typically C–O and S–O photoelectron lines are found at binding energies (BEs) of 289 and 169 eV, respectively) (74). Shown in Figure 2e–h are the spectra obtained from an identical sample that was stored in air for 1 month. In this case only minor differences were observed. As shown, trace oxidation was detected in the C(1s) and S(2p) spectra, testifying to the robustness of the thienylsilane molecular layer. As an additional means for characterization of the thienylsilane molecular layer, the Kelvin probe estimated work function of the surface was found to be 4.77 eV. This result is in agreement with other molecular layers bearing aromatic groups on ITO substrates (75).

Electrochemical Deposition of ePEDOT:PSS. Using the discussed ITO-coated glass samples as a working electrode in a standard three-electrode electrochemical cell,

Table 1. Atomic Concentrations (%) As Determined by AR-XPS at Various Takeoff Angles[a]

takeoff angle (deg)	In (3d)	Sn (3d)	O (1s)	C (1s)	S (2p)	Si (2p)
90	23.03	3.48	46.66	20.12	3.07	3.64
45	20.44	3.40	44.26	24.60	3.08	4.22
15	14.87	2.88	36.80	36.85	3.17	5.42

[a] Lower takeoff angles provide chemical information from a limited region located near the sample surface.

we were able to study the utility of the thienylsilane molecular layer as an improved interface for electrochemically deposited poly(3,4-ethylenedioxythiophene:poly(*p*-styrenesulfonate) (ePEDOT:PSS). Our approach involves a quantitative analysis of potentiodynamic cyclic voltammetric experiments with differing maximum applied potentials (V_{max}) so as to conclusively determine key electrochemical differences and criteria for the electrodeposition of these films from aqueous PSSNa electrolyte.

ePEDOT:PSS was deposited by sweeping the working electrode potential from −1.00 V to $+V_{max}$ (vs Ag/Ag^+) at 100 mV/s for a specified number of cycles. Representative cyclic voltammetric sweeps showing the growth of ePEDOT:PSS on hydroxy- and thienylsilane-functionalized ITO working electrodes are shown in Figure 3a−c and Figure 3d−f, respectively. Characteristic broad redox waves with increasing anodic and cathodic peak currents for each successive cycle are evidence for the growth of ePEDOT:PSS. Additionally, during the experiment a light blue film became visible on the ITO electrodes. Trends within a series (a−c or d−f) are also present. With decreasing V_{max}, a decrease in the area beneath each curve is evident, indicating a decrease in the amount of electrochemically addressable ePEDOT:PSS film. This is consistent with the decreasing difference in anodic and cathodic peak currents with decreasing V_{max}. These trends continue within each series until the critical V_{max} required for the potentiodynamic deposition of ePEDOT:PSS is not exceeded. In the case of the hydroxy-functionalized ITO working electrodes, no ePEDOT:PSS film was obvious at potentials below 1.00 V. For the thienylsilane-functionalized ITO analogue, this limiting potential was at a lower value of 0.85 V. These differences in polymerization onset potential are also consistent with the variations in surface work function measured by Kelvin probe. The thienylsilane-modified surfaces had measured work functions significantly lower than the values measured for unmodified ITO. This difference indicates that the extraction of electrons from the modified surfaces requires less driving energy, and electropolymerization should proceed at a reduced electrical potential. Furthermore, it is known that the primary nucleation steps of electrochemical depositions typically require higher potentials than the growth steps. As observed by others, the monomeric units within the molecular layer act as favorable nucleation sites for electrochemical polymerization and hence result in a surface requiring lower electrical potential for nucleation (46, 50, 76, 77). It is likely that the resulting ePEDOT:PSS film propagates from the thienylsilane

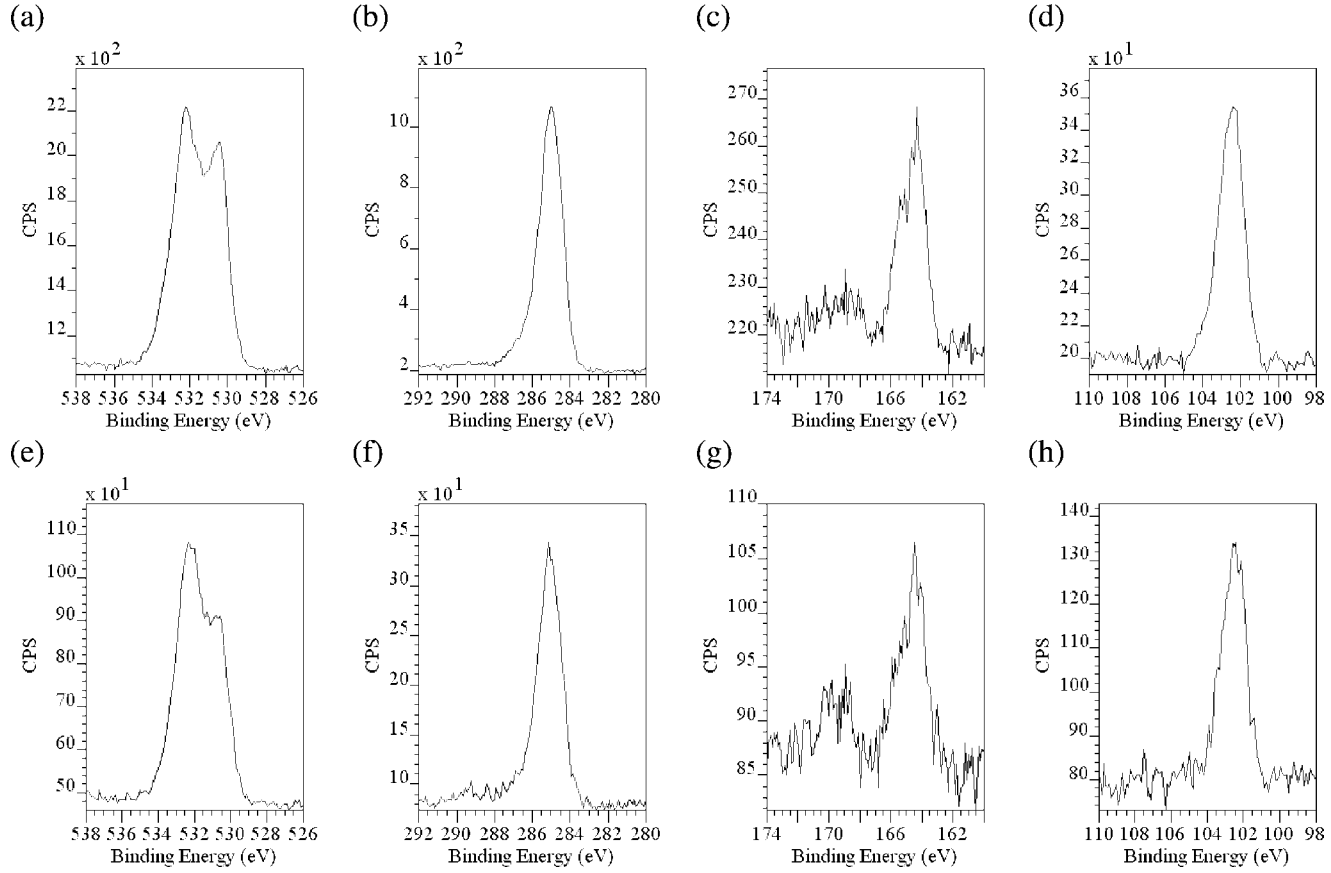

FIGURE 2. High-resolution XPS spectra of O(1s), C(1s), S(2p), and Si(2p) for thienylsilane-modified ITO-coated glass: (a−d) as synthesized; (e−h) following 4 weeks of exposure to air. In all cases the takeoff angle was 15°. On the *y* axis, CPS denotes counts per second.

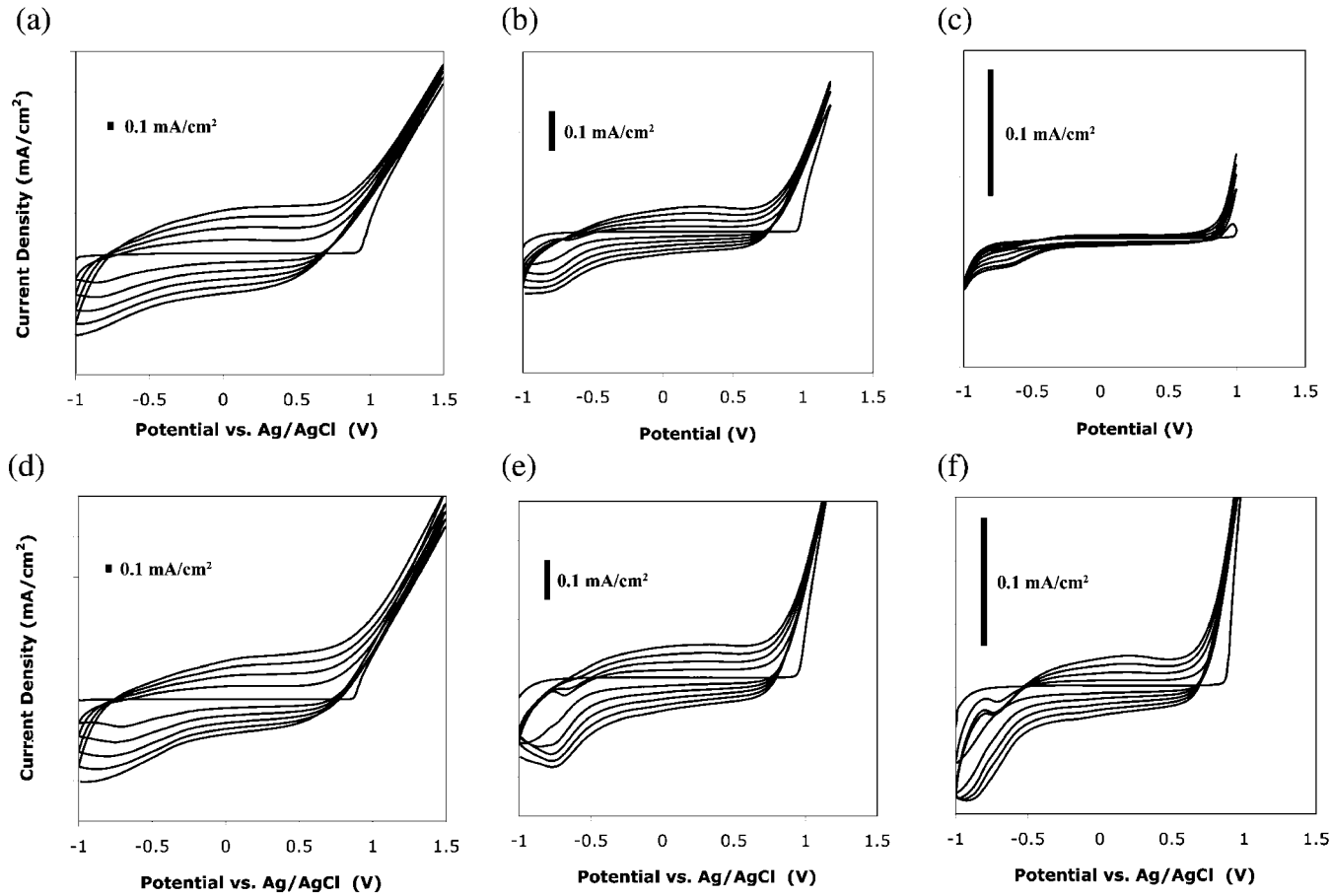

FIGURE 3. Five consecutive cyclic voltammetric sweeps for the electrochemical growth of ePEDOT:PSS: (a–c) on hydroxy-functionalized ITO; (d–f) on thienylsilane-functionalized ITO. The maximum applied potentials in a–f were 1.50, 1.20, 1.00, 1.50, 1.20, and 1.00 V, respectively. A scan rate of 100 mV/s was used, and the initial concentrations of 3,4-ethylenedioxythiophene and poly(*p*-styrenesulfonate) were 10 and 20 mM, respectively.

units by way of a covalent linkage, which also suggests that improvements in the cross-sectional conductivity of the film would result (see discussion below).

For a more quantitative analysis and comparison of each series, the area-normalized charge for each cycle was determined. The plots of the charge density transferred using hydroxy- and thienylsilane-functionalized ITO working electrodes versus cycle number are depicted in parts a and b of Figure 4, respectively. In Figure 4a, there is no significant rate of increase in the charge transferred until V_{max} exceeds 1.00 V, suggesting negligible ePEDOT:PSS growth. Comparatively, in Figure 4b this feature occurs at a lower value, ~0.85 V, suggesting that the presence of a thienylsilane molecular layer facilitates film growth by providing additional nucleation sites. Beyond these limiting potentials, both cases exhibit increasing slopes to the curves, indicating higher rates of film growth at greater V_{max} values. In all cases the rates of ePEDOT:PSS growth are higher for the thienylsilane-functionalized ITO working electrode, perhaps due to initial nucleation of the film over larger areas of the electrode. The degree of linearity in Figure 4 is also noteworthy. When they are compared, data sets in Figure 4b maintain linearity to higher cycle number than in Figure 4a. A possible explanation for the deviation from linearity is that, with ongoing potentiodynamic deposition, the rate of growth of the ePEDOT:PSS film is becoming increasingly uncontrolled, leading to increasing rates of polymer growth by way of increasing surface area and, hence, an increase in the surface roughness is expected. This argument is supported by previous studies that have found that the growth of polythiophene films extend from complex nucleation at the electrode as well as within the growing film (78). The curvature of the plots in Figure 4, therefore, suggest that thienylsilane molecular layers allow for a uniform growth of ePEDOT:PSS mainly by way of propagation from covalently tethered ePEDOT chains.

Physical and Electrical Characterization ePEDOT:PSS Films. The results of the electrochemical deposition of ePEDOT:PSS using a thienylsilane molecular layer are expected to lead to significant differences in the films' properties. Improvements in adhesion, surface roughness, and electrical conductivity are expected. To characterize these features, we investigated surface adhesion by a Scotch tape test and scanning force microscopy. Additionally, to quantify the electrical properties, samples were produced using a potentiostatic approach at applied potentials within the range of those discussed above. Films produced in this manner are therefore isolated in the highly conductive state and are most relevant as anodes for polymer photovoltaic solar cells. In addition to a macroscopic investigation (see

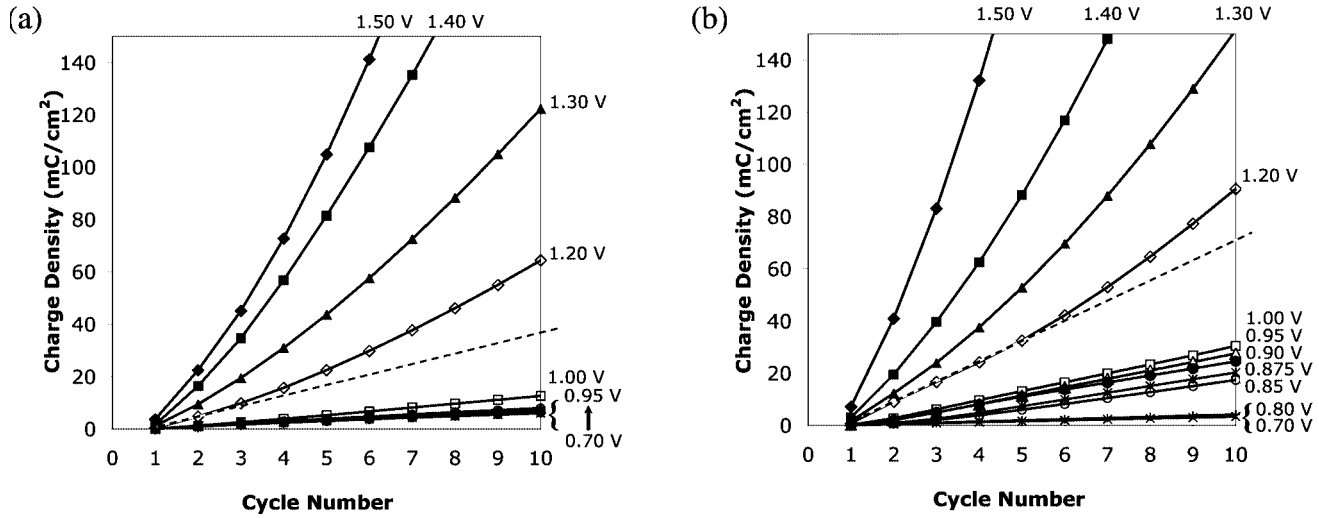

FIGURE 4. Charge density, obtained from the anodic waves of potentiodynamic experiments, versus the cycle number for hydroxy-functionalized ITO (a) and thienylsilane-functionalized ITO working electrodes (b). A scan rate of 100 mV/s was used, and the initial concentrations of 3,4-ethylenedioxythiophene and poly(*p*-styrenesulfonate) were 10 and 20 mM, respectively. The dotted lines are included as references for linearity.

the Supporting Information), we characterized the conductivity of the samples using conducting probe scanning force microscopy (CP-SFM). In both cases the "through-film" electrical characteristics are determined. This technique also permits characterization of the uniformity of the electrical conductivity where the presence of "hotspots" of high conduction are easily visualized (55, 61, 79).

The electrochemical growth of ePEDOT:PSS from a thienylsilane molecular layer led to improved adhesion of the resulting film relative to the hydroxyl-terminated ITO substrates. This was determined by placing a piece of Scotch tape onto the samples followed by removal and visually inspecting the resulting quality of films. In the case of ePEDOT:PSS grown on modified ITO, the film appearance was unchanged, whereas those grown on hydroxy-functionalized ITO showed strong evidence of delamination. As discussed earlier, more uniform ePEDOT:PSS growth rates were observed for thienylsilane-functionalized electrodes, suggesting improvement of both nucleation and film growth. Shown in Figure 5a–d and Figure 5e–h are representative scanning force microscopy (SFM) images of ePEDOT:PSS prepared using hydroxy- and thienylsilane-functionalized ITO, respectively. A 15 s potentiostatic deposition of a ePEDOT:PSS film at 1.05 V on hydroxy-ITO (a potential slightly higher than the limiting potential required for electrochemical deposition, Figure 5a) clearly shows isolated nucleation and growth of island features with 100 nm height, up to 300 nm in diameter. In contrast, the thienylsilane-functionalized ITO (Figure 5e) is much smoother and has roughness similar to that of the unmodified ITO substrate (Figure 5i). While subtle, the SFM series of ePEDOT:PSS films (20–30 nm) potentiostatically grown at higher potentials of 1.15, 1.25, and 1.35 V consistently reveal small islandlike features (~50–100 nm diameter) on the hydroxy-terminated ITO that are not visible on the thienylsilane-terminated ITO. As with the 1.05 V case, the roughness of the layers grown with the thienyl surface (rms roughness ~4.8 nm) is more similar to that of the starting ITO (rms ~5.0 nm, see the Supporting Information). Functionalization of the ITO surface seems, therefore, to result in a more uniform primary nucleation step in the early stages of electrodeposition (55, 61, 79, 80). Similar results for electrodeposited polythiophenes on thienylalkylsilane-modified ITO electrodes have also recently been observed (50, 77).

As a means for the chemical characterization of the ePEDOT:PSS film, we acquired the surface O(1s), C(1s), and S(2p) XPS spectra for a film grown using a thienylsilane-functionalized ITO substrate (parts a–c of Figure 6, respectively). Due to the complex nature of the ePEDOT:PSS blend, multicomponent spectra result. Previous efforts have identified that the O(1s) spectrum is composed of four distinct chemical species that are easily deconvoluted (60). A peak at 531.9 eV corresponds to the oxygen in sulfonate residues of the PSSNa, whereas S═O and S–OH for the sulfonic acid (PSSH) groups are resolved at approximately 532.4 and 533.4 eV, respectively (81). The final peak at a BE value of 533.7 eV corresponds to oxygen incorporated as ether groups within ePEDOT. Deconvolution of the O(1s) spectra therefore permits an estimate of the ePEDOT:PSS molar ratio. We have determined this value to be ~1.5, concluding that the surface of the film has a significant contribution of the high-conductivity PEDOT component. Since commercially available PEDOT:PSS typically has a molar ratio of ~0.83 (82), we anticipate very good electrical conductivity through the ePEDOT:PSS film. The C(1s) spectra had two main features, a high BE peak at 286.5 eV and a lower BE peak at 285.0 eV. The former is assigned to the saturated and π-conjugated carbon atoms in the ePEDOT and PSS, whereas the latter peak is the signal from C–O–C bonds in the PEDOT (83). Deconvolution of the S(2p) spectra in Figure 6c was not possible, due to the presence of up to eight components in this region (84). Roughly summarizing, doublets at ~164.0 and 168.2 eV correspond to sulfur in the ePEDOT and PSS, respectively. Last, and as an additional means for characterization, we determined the Kelvin probe estimated work function of the ePEDOT:PSS films grown

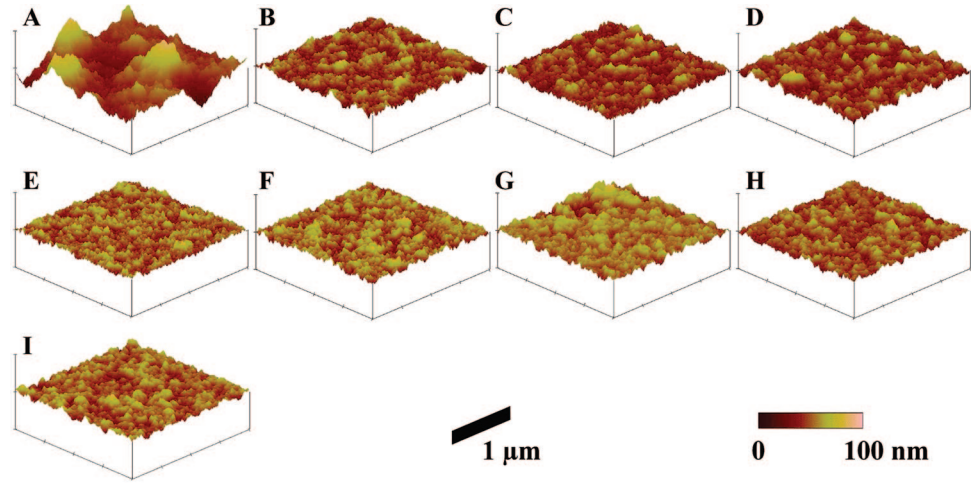

FIGURE 5. Scanning force microscopy images of ePEDOT:PSS grown potentiostatically for 15 s using (A−D) hydroxy-functionalized and (E−H) thienylsilane functionalized ITO working electrodes. Applied potentials: (A) 1.05 V; (B) 1.15 V; (C) 1.25 V; (D) 1.35 V; (E) 1.05 V; (F) 1.15 V; (G) 1.25 V; (H) 1.35 V. The initial concentrations of 3,4-ethylenedioxythiophene and poly(*p*-styrenesulfonate) were 10 and 20 mM, respectively. (I) Unmodified ITO.

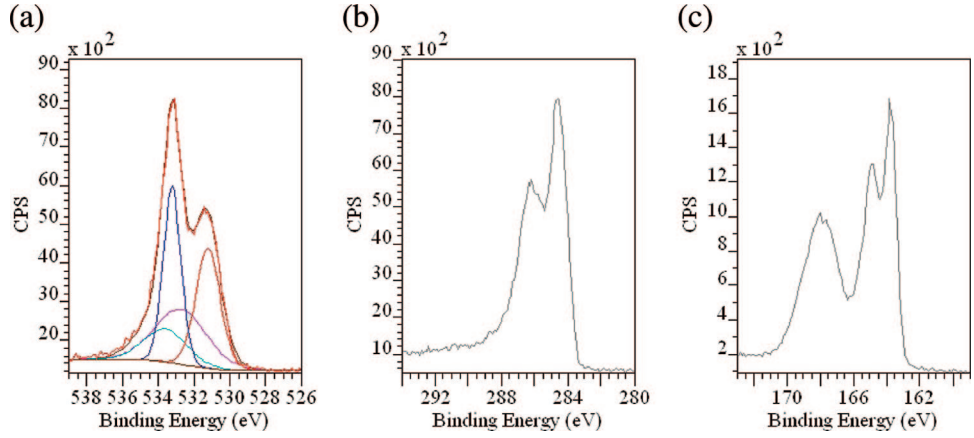

FIGURE 6. High-resolution XPS spectra of (a) O(1s), (b) C(1s), and (c) S(2p) for ePEDOT:PSS electrochemically deposited using a thienylsilane modified ITO-coated electrode. The takeoff angle was 90°.

using hydroxy- and thienylsilane-functionalized ITO. The respective values, 4.89 and 4.87 eV, were within experimental uncertainty of one another but significantly different from the initial values of the electrodes.

The electrical conductivity of ePEDOT:PSS was investigated by CP-SFM. An applied bias range of 0−500 mV was used to quantify the average current passed through the ePEDOT:PSS films over 4 μm^2 areas (see the Supporting Information). Shown in Figure 7a,d are the area-averaged *I* vs *V* curves for ePEDOT:PSS potentiostatically deposited on hydroxy- and thienylsilane-functionalized ITO electrodes, respectively (60 s deposition). Both plots exhibit linearity in the potential range (0−500 mV), confirming that the electrical contacts are ohmic. The key difference, however, is that the ePEDOT:PSS films grown using the thienylsilane-functionalized electrodes display current values that are approximately an order of magnitude larger than for the hydroxy-ITO analogues. For a more accurate comparison, the thickness of the electrodeposited films was determined. Shown in Figure 7b,e are the plots describing the thickness of the films as a function of the potentiostatic potential used for the electrochemical deposition. In the case of hydroxy-ITO working electrodes, it seems that the growth of thicker ePEDOT:PSS films is favored for potentiostatic potentials near 1.35 V. Interestingly, the corresponding value for the thienylsilane derivative is 1.25 V. Equation 1 describes the relationship for potential (*V*), current (*I*), film thickness, (d) and the resistivity per unit area (ρ/A):

$$V = Id \times (\rho / A) \quad (1)$$

Assuming that the electrical contacts for these measurements are ohmic, a plot of *Id* vs *V* therefore represents a normalized plot for which film thickness values are accounted. Shown in Figure 7c,f are the corresponding plots. Again, in spite of the film thickness, the conductivity of ePEDOT:PSS electrosynthesized using thienylsilane-modified electrodes is improved by a factor of ~6 (for a consistent 1 cm^2 area comparison, see the Supporting Information). As documented by others, we attribute the increased conductivity to the improved charge transfer between the electrode and polymer (85). The most conductive ePEDOT:PSS grown on thienylsilane-modified ITO was deposited at a potentiostatic value of 1.15 V.

Bulk Heterojunction Photovoltaic Devices. The effect of thienylsilane surface modification over the performance of bulk heterojunction organic photovoltaic solar cells

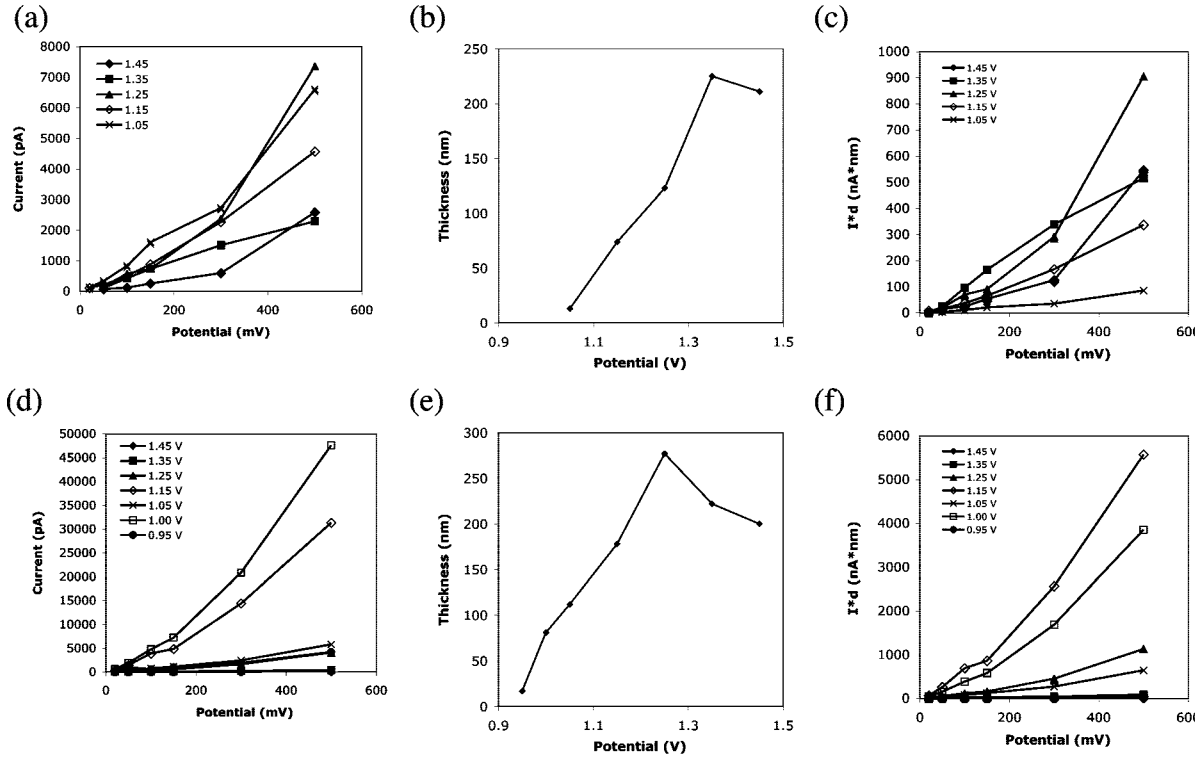

FIGURE 7. Summary of electrical characteristics for electrochemically prepared ePEDOT:PSS using (a–c) hydroxy- and (d–f) thienylsilane-functionalized ITO electrodes. Parts a and d are the current versus potential curves for ePEDOT:PSS prepared at differing potentiostatic values. Parts b and e are the film thickness profiles for the same films as determined by a SFM image of scratched areas. Parts c and f describe the electrical conductivity as a function of the polymerization potential.

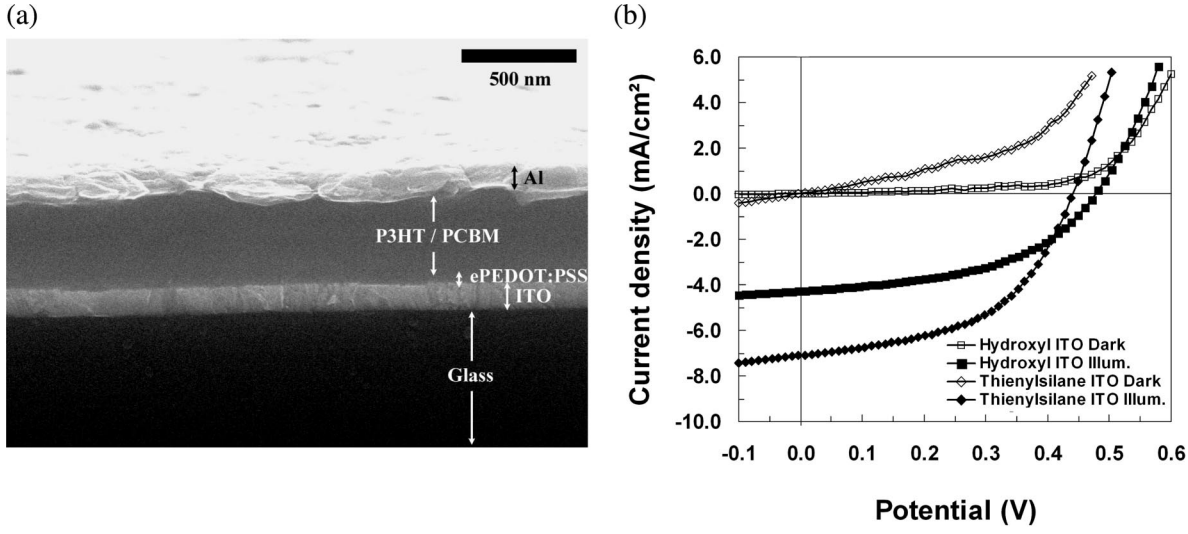

FIGURE 8. (a) Cross-sectional SEM image of a P3HT/PCBM bulk heterojunction photovoltaic device fabricated with thienylsilane-functionalized ITO. (b) Dark (open symbols) and illuminated (Illum., solid symbols) *J*/*V* plots for a BHJ OPV device fabricated with hydroxyl- and thienylsilane-functionalized ITO anodes. For clarity we have suggested the ePEDOT:PSS location in (a) due to insufficient contrast between the active layer and the ePEDOT:PSS layers.

was investigated using the standard P3HT/PCBM active layer system. Two sets of devices were prepared, one with thienylsilane-modified ITO electrodes and a control series with unmodified ITO. Overall device configurations were as follows: (i) ITO/ePEDOT:PSS (30 nm, 1.15 V, 15 s)/P3HT + PCBM (300 nm)/Al (120 nm) and (ii) ITO/thienylsilane/ePEDOT:PSS (30 nm, 1.15 V, 15 s)/P3HT + PCBM (300 nm)/Al (120 nm). A cross-sectional scanning electron micrograph of device ii is shown in Figure 8a. In the image, distinct regions associated with the glass substrate, ITO electrode, active region, and Al top contact are easily resolved, and these materials are marked on the figure. In the active region, insufficient atomic number or textural contrast is available to readily identify interfaces among ePEDOT:PSS, P3HT, PCBM, and thienylsilane. For clarity we have included the expected location of the ePEDOT:PSS in Figure 8a.

A comparison of the dark and illuminated (AM 1.5 G simulated irradiance) current density–voltage (*J*–*V*) curves for representative devices is shown in Figure 8b. The averaged performance characteristics for six devices from each

Table 2. Summary of P3HT/PCBM Bulk Heterojunction Photovoltaic Device Characteristics[a]

ITO substrate	J_{sc}, mA/cm^2 (std dev)	V_{oc}, V (std dev)	FF (std dev)	η, % (std dev)
hydroxyl	4.44 (0.76)	0.49 (0.03)	0.42 (0.04)	0.96 (0.14)
thienylsilane	6.81 (0.43)	0.43 (0.02)	0.49 (0.03)	1.51 (0.17)

[a] All values are the average of six 0.12 cm^2 devices.

series are summarized in Table 2. The short-circuit current density (J_{sc}) was found to be significantly greater in the device fabricated with a thienylsilane-modified anode. A reduced open-circuit potential (V_{oc}) and an increase in the fill factor (FF) of the devices was also found. Correspondingly, the power conversion efficiency (η) of devices fabricated with thienylsilane-modified anodes ($\eta = 1.5\%$) was found to be greater than for control samples prepared under identical conditions without surface-modified substrates ($\eta = 1.0\%$). These observations are consistent with the behavior of copper phthalocyanine (CuPc)/fullerene planar junction devices investigated with and without thiophene acetic acid interfacial-modification layers (46). It is expected that the improved electrical and morphological characteristics of ePEDOT:PSS deposited over thienylsilane-functionalized ITO electrodes allows improved charge transfer through the photovoltaic device and, therefore, creates a significant improvement in the photocurrent extraction from the device. As a consequence, a relative improvement in device efficiency is measured using thienylsilane interfacial modification layers over devices prepared from standard ITO substrates.

CONCLUSIONS

The vapor-phase functionalization of freshly cleaned ITO surfaces with triethoxy-2-thienylsilane affords a stable molecular layer. The thienylsilane-modified ITO electrode was effective at reducing the onset polymerization potential required for the electrochemical deposition of 3,4-ethylenedioxythiophene from poly(*p*-styrenesulfonate) electrolyte. Films fabricated by these means were generally found to be smoother and more uniform than the counterparts synthesized using the parent ITO electrode. XPS investigations of the ePEDOT:PSS determined that the topmost surface was rich in the conductive PEDOT component and high through-film conductivity was found by CP-SFM. When thienylsilane-modified ITO electrodes were used as anodes (rather than bare ITO analogues) in P3HT/PCBM BHJ solar cells, a relative improvement in the device efficiency was observed, which we propose is due to improved charge transfer across the ePEDOT:PSS/ITO boundary via surface tethered thiophene units.

Acknowledgment. This work was supported by the Natural Sciences and Engineering Research Council of Canada (NSERC), NRC-NINT, the University of Alberta, the Canadian Foundation for Innovation (CRC to J.M.B. and M.J.B.), the Informatics Circle of Research Excellence (iCORE), and Micralyne, Inc. D.A.R. acknowledges the Killam Foundation for a PDF. Dr. Dimitre Karpuzov and his colleagues at the Alberta Centre for Surface Engineering and Science (ACSES) are thanked for their considerable assistance with XPS techniques. Dr. Richard McCreery is acknowledged for providing access to Kelvin probe equipment.

Supporting Information Available: Figures and tables giving CP-SFM current images of electropolymerized PEDOT:PSS on hydroxy- and thienylsilane-modified ITO electrodes, a macroscopic conductivity comparison, and P3HT/PCBM bulk heterojunction photovoltaic device characterization. This material is available free of charge via the Internet at http://pubs.acs.org.

REFERENCES AND NOTES

(1) Tang, C. W. *Appl. Phys. Lett.* **1986**, *48*, 183–184.
(2) Sariciftci, N. S.; Smilowitz, L.; Heeger, A. J.; Wudl, F. *Science* **1992**, *258*, 1474–1476.
(3) Yu, G.; Pakbaz, K.; Heeger, A. J. *Appl. Phys. Lett.* **1994**, *64*, 3422–3424.
(4) Halls, J. J. M.; Walsh, C. A.; Greenham, N. C.; Marseglia, E. A.; Friend, R. H.; Moratti, S. C.; Holmes, A. B. *Nature* **1995**, *376*, 498–500.
(5) Brabec, C. J.; Cravino, A.; Meissner, D.; Sariciftci, N. S.; Fromherz, T.; Rispens, M. T.; Sanchez, L.; Hummelen, J. C. *Adv. Funct. Mater.* **2001**, *11*, 374–380.
(6) Shaheen, S. E.; Radspinner, R.; Peyghambarian, N.; Jabbour, G. E. *Appl. Phys. Lett.* **2001**, *79*, 2996–2998.
(7) Xue, J.; Uchida, S.; Rand, B. P.; Forrest, S. R. *Appl. Phys. Lett.* **2004**, *84*, 3013–3015.
(8) Coakley, K. M.; McGehee, M. D. *Chem. Mater.* **2004**, *16*, 4533–4542.
(9) Spanggaard, H.; Krebs, F. C. *Sol. Energy Mater. Sol. Cells* **2004**, *83*, 125–146.
(10) Roncali, J. *Chem. Soc. Rev.* **2005**, *34*, 483–495.
(11) Gledhill, S. E.; Scott, B.; Gregg, B. A. *J. Mater. Res.* **2005**, *20*, 3167–3179.
(12) Blom, P. W. M.; Mihailetchi, V. D.; Koster, L. J. A.; Markov, D. E. *Adv. Mater.* **2007**, *19*, 1551–1566.
(13) Krebs, F. C.; Spanggard, H.; Kjaer, T.; Biancardo, M.; Alstrup, J. *Mater. Sci. Eng., B* **2007**, *138*, 106–111.
(14) Lungenschmied, C.; Dennler, G.; Neugebauer, H.; Sariciftci, N. S.; Glatthaar, M.; Meyer, T.; Meyer, A. *Sol. Energy Mater. Sol. Cells* **2007**, *91*, 379–384.
(15) Saunders, B. R.; Turner, M. L. *Adv. Coll. Inter. Sci.* **2008**, *138*, 1–23.
(16) Thompson, B. C.; Fréchet, J. M. *Angew. Chem., Int. Ed.* **2008**, *47*, 58–77.
(17) Günes, S.; Neugebauer, H.; Sariciftci, N. S. *Chem. Rev.* **2007**, *107*, 1324–1338.
(18) Kim, J. Y.; Lee, K.; Coates, N. E.; Moses, D.; Nguyen, T.-Q.; Dante, M.; Heeger, A. J. *Science* **2007**, *317*, 222–225.
(19) Li, G.; Shrotriya, V.; Huang, J.; Yao, Y.; Moriarty, T.; Emery, K.; Yang, Y. *Nat. Mater.* **2005**, *4*, 864–868.
(20) Yu, G.; Gao, J.; Hummuelen, J. C.; Wudl, F.; Heeger, A. J. *Science* **1995**, *270*, 1789–1791.
(21) Ma, W.; Yang, C.; Gong, X.; Lee, K.; Heeger, A. J. *Adv. Funct. Mater.* **2005**, *15*, 1617–1622.
(22) Reyes-Reyes, M.; Kim, K.; Dewald, J.; Lopez-Sandoval, R.; Avadhanula, A.; Curran, S.; Carroll, D. L. *Org. Lett.* **2005**, *7*, 5749–5752.
(23) Yang, X.; Loos, J.; Veenstra, S. C.; Verhees, W. J. H.; Wienk, M. M.; Kroon, J. M.; Michels, M. A. J.; Janssen, R. A. J. *Nano Lett.* **2005**, *5*, 579–583.
(24) Kim, J. Y.; Kim, S. H.; Lee, H.-H.; Lee, K.; Ma, W.; Gong, X.; Heeger, A. J. *Adv. Mater.* **2006**, *18*, 572–576.
(25) Xin, H.; Kim, F. S.; Jenekhe, S. A. *J. Am. Chem. Soc.* **2008**, *130*, 5424–5425.
(26) van Bavel, S. S.; Sourty, E.; de With, G.; Loos, J. *Nano Lett.* ASAP.

(27) Li, G.; Shrotriya, V.; Yao, Y.; Huang, J.; Yang, Y. *J. Mater. Chem.* **2007**, *17*, 3126–3140.
(28) Mayer, A. C.; Scully, S. R.; Hardin, B. E.; Rowell, M. W.; McGehee, M. D. *Mater. Today* **2007**, *10*, 28–33.
(29) Winder, C.; Sariciftci, N. S. *J. Mater. Chem.* **2004**, *14*, 1077–1086.
(30) Bundgaard, E.; Krebs, F. C. *Sol. Energy Mater. Sol. Cells* **2007**, *91*, 954–985.
(31) Peet, J.; Kim, J. Y.; Coates, N. E.; Ma, W. L.; Moses, D.; Heeger, A. J.; Bazan, G. C. *Nat. Mater.* **2007**, *6*, 497–500.
(32) Kroon, R.; Lenes, M.; Hummelen, J. C.; Blom, P. W. M.; de Boer, B. *Polym. Rev.* **2008**, *48*, 531–582.
(33) Yoo, S.; Potscavage, W. J.; Domercq, B.; Kim, J.; Holt, J.; Kippelen, B. *Appl. Phys. Lett.* **2006**, *89*, 233516.
(34) Moule, A. J.; Bonekamp, J. B.; Meerholz, K. *J. Appl. Phys.* **2006**, *100*, 094503.
(35) Kim, Y.; Cook, S.; Tuladhar, S. M.; Choulis, S. A.; Nelson, J.; Durrant, J. R.; Bradley, D. D. C.; Giles, M.; McCulloch, I.; Ha, C.-S.; Ree, M. *Nat. Mater.* **2006**, *5*, 197–203.
(36) Padinger, F.; Rittberger, R. S.; Sariciftci, N. S. *Adv. Funct. Mater.* **2003**, *13*, 85–88.
(37) Waldauf, C.; Schilinsky, P.; Hauch, J.; Brabec, C. J. *Thin Solid Films* **2004**, *451–452*, 503–507.
(38) Krebs, F. C.; Norrman, K. *Prog. Photovolt.: Res. Appl.* **2007**, *15*, 697–712.
(39) Krebs, F. C. *Sol. Energy Mater. Sol. Cells* **2008**, *92*, 715–726.
(40) Jørgensen, M.; Norrman, K.; Krebs, F. C. *Sol. Energy Mater. Sol. Cells* **2008**, *92*, 686–714.
(41) Hauch, J. A.; Schilinsky, P.; Choulis, S. A.; Childers, R.; Biele, M.; Brabec, C. J. *Sol. Energy Mater. Sol. Cells* **2008**, *92*, 727–731.
(42) Sirringhaus, H.; Tessler, N.; Friend, R. H. *Science* **1998**, *280*, 1741–1744.
(43) Ravirajan, P.; Peiro, A. M.; Nazeeruddin, M. K.; Graetzel, M.; Bradley, D. D. C.; Durrant, J. R.; Nelson, J. *J. Phys. Chem. B* **2006**, *110*, 7635–7639.
(44) Goh, C.; Scully, S. R.; McGehee, M. D. *J. Appl. Phys.* **2007**, *101*, 114503.
(45) Murray, R. W. *Molecular Design of Electrode Surfaces*; Wiley: New York, 1992; Vol. 22.
(46) Armstrong, N. R.; Carter, C.; Donley, C.; Simmonds, A.; Lee, P.; Brumbach, M.; Kippelen, B.; Domercq, B.; Yoo, S. *Thin Solid Films* **2003**, *445*, 342–352.
(47) Veinot, J. G. C.; Marks, T. J. *Acc. Chem. Res.* **2005**, *38*, 632–643.
(48) Sullivan, J. T.; Harrison, K. E.; Mizzell, J. P.; Kilbey, S. M., II *Langmuir* **2000**, *16*, 9797–9803.
(49) Marrikar, F. S.; Brumbach, M.; Evans, D. H.; Lebron-Paler, A.; Pemberton, J. E.; Wysocki, R. J.; Armstrong, N. R. *Langmuir* **2007**, *23*, 1530–1542.
(50) Hwang, E.; de Silva, K. M. N.; Seevers, C. B.; Li, J. R.; Garno, J. C.; Nesterov, E. E. *Langmuir* **2008**, *24*, 9700–9706.
(51) Roman, L. S.; Mammo, W.; Pettersson, L. A. A.; Andersson, M. R.; Inganäs, O. *Adv. Mater.* **1998**, *10*, 774–777.
(52) Brabec, C. J.; Shaheen, S. E.; Winder, C.; Sariciftci, N. S.; Denk, P. *Appl. Phys. Lett.* **2002**, *80*, 1288–1290.
(53) Granström, M.; Petritsch, K.; Arias, A. C.; Lux, A.; Andersson, M. R.; Friend, R. H. *Nature* **1998**, *395*, 257–260.
(54) Peumans, P.; Forrest, S. R. *Appl. Phys. Lett.* **2001**, *79*, 126–128.
(55) Kemerink, M.; Timpanaro, S.; de Kok, M. M.; Meulenkamp, E. A.; Touwslager, F. J. *J. Phys. Chem. B* **2004**, *108*, 18820–18825.
(56) Crispin, X.; Marciniak, S.; Osikowicz, W.; Zotti, G.; Denier Van Der Gon, A. W.; Louwet, F.; Fahlman, M.; Groenendaal, L.; de Schryver, F.; Salaneck, W. R. *J. Polym. Sci. B: Polym. Phys.* **2003**, *41*, 2561–2583.
(57) Kirchmeyer, S.; Reuter, K. *J. Mater. Chem.* **2005**, *15*, 2077–2088.
(58) Han, D. H.; Kim, J. W.; Park, S. M. *J. Phys. Chem. B* **2006**, *110*, 14874–14880.
(59) Pingree, L. S. C.; MacLeod, B. A.; Ginger, D. S. *J. Phys. Chem. C* **2008**, *112*, 7922–7927.
(60) Greczynski, G.; Kugler, T.; Salaneck, W. R. *Thin Solid Films* **1999**, *354*, 129–135.
(61) Nardes, A. M.; Kemerink, M.; Janssen, R. A. J.; Bastiaansen, J. A. M.; Kiggen, N. M. M.; Langeveld, B. M. W.; van Breemen, A. J. J. M.; de Kok, M. M. *Adv. Mater.* **2007**, *19*, 1196–1200.
(62) Baikie, I. D.; Estrup, P. J. *Rev. Sci. Instrum.* **1998**, *69*, 3902–3907.
(63) Hansen, W. N.; Hansen, G. J. *Surf. Sci.* **2001**, *481*, 172–184.
(64) de Jong, M. P.; van Ijzendoorn, L. J.; de Voigt, M. J. A. *Appl. Phys. Lett.* **2000**, *77*, 2255–2257.
(65) Donley, C.; Dunphy, D.; Paine, D.; Carter, C.; Nebesny, K.; Lee, P.; Alloway, D.; Armstrong, N. R. *Langmuir* **2002**, *18*, 450–457.
(66) We have confirmed a substantial surface hydroxyl group content for ITO on glass by adsorption of $Fc(COOH)_2$ from 0.20 M ethanol solution. Quantification of the surface density of redox-active ferrocene moieties was achieved by cyclic voltammetry where integration of the anodic peaks for the ferrocenyl/ferroceniumyl redox couple were used. This method confirmed an areal density of adsorbed $Fc(COOH)_2$ of $\sim 1.7 \times 10^{-10}$ mol cm^{-2}. For further details on this method please see: Zotti, G.; Schiavon, G.; Zecchin, S.; Berlin, A.; Ragani, G. *Langmuir* **1998**, *14*, 1728–1733.
(67) Milliron, D. J.; Hill, I. G.; Shen, C.; Kahn, A.; Schwartz, J. *J. Appl. Phys.* **2000**, *87*, 572–576.
(68) Malinsky, J. E.; Veinot, J. G. C.; Jabbour, G. E.; Shaheen, S. E.; Anderson, J. D.; Lee, P.; Richter, A. G.; Burin, A. L.; Ratner, M. A.; Marks, T. J.; Armstrong, N. R.; Kippelen, B.; Dutta, P.; Peyghambarian, N. *Chem. Mater.* **2002**, *14*, 3054–3065.
(69) Cho, J. H.; Kim, J. W.; Kim, K. S.; Lee, W. Y.; Kim, S. H.; Choi, W. Y. *Key Eng. Mat.* **2005**, *297–300*, 2351–2355.
(70) Zuppiroli, L.; Si-Ahmed, L.; Kamaras, K.; Nuesch, F.; Bussac, M. N.; Ades, D.; Siove, A.; Moons, E.; Grätzel, M. *Eur. Phys. J. B* **1999**, *11*, 505–512.
(71) Cossement, D.; Plumier, F.; Delhalle, J.; Hevesi, L.; Mekhalif, Z. *Synth. Met.* **2003**, *138*, 529–536.
(72) The signal intensity detected using this technique arises from a depth d defined by the relation $d = \lambda \sin \theta$, where the electron takeoff angle is θ and the mean free path of the ejected electron is λ. Therefore, for low values in θ, the photoelectron signal is anticipated to arise from the topmost region of the sample.
(73) Harrison, K. E.; Kang, J. F.; Haasch, R. T.; Kilbey, S. M., II *Langmuir* **2001**, *17*, 6560–6568.
(74) Moulder, J. F.; Stickle, W. F.; Sobol, P. E.; Bomden, K. D. *Handbook of X-ray Photoelectron Spectroscopy: A Reference Interpretation of XPS Data*; Perkin-Elmer Corp.: Eden Prairie, MN, 1992.
(75) Ganzorig, C.; Kwak, K.-J.; Yagi, K.; Fujihira, M. *Appl. Phys. Lett.* **2001**, *79*, 272–274.
(76) Kim, N. Y.; Laibinis, P. E. *J. Am. Chem. Soc.* **1999**, *121*, 7162–7163.
(77) Kang, J. F.; Perry, J. D.; Tian, P.; Kilbey, S. M., II *Langmuir* **2002**, *18*, 10196–10201.
(78) Hamnett, A.; Hillman, A. R. *J. Electrochem. Soc.* **1988**, *135*, 2517–2524.
(79) Ionescu-Zanetti, C.; Mechler, A.; Carter, S. A.; Lal, R. *Adv. Mater.* **2004**, *16*, 385–389.
(80) del Valle, M. A.; Cury, P.; Schrebler, R. *Electrochem. Acta* **2002**, *48*, 397–405.
(81) Zotti, G.; Zecchin, S.; Schiavon, G.; Louwet, F.; Groenendaal, L.; Crispin, X.; Osikowicz, W.; Salaneck, W.; Fahlman, M. *Macromolecules* **2003**, *36*, 3337–3344.
(82) Bayer, Baytron P Product Information.
(83) Lee, C. S.; Joo, J.; Han, S.; Lee, J. H.; Koh, S. K. *J. Kor. Phys. Soc.* **2004**, *45*, 747–750.
(84) Nguyen, T. P.; Le Rendu, P.; Long, P. D.; De Vos, S. A. *Surf. Coat. Technol.* **2004**, *180*, 646–649.
(85) Vermeir, I. E.; Kim, N. Y.; Laibinis, P. E. *Appl. Phys. Lett.* **1999**, *74*, 3860–3862.

AM800081K